Heterogeneous & Homogeneous & Bio- & Nano-
CHEMCATCHEM
CATALYSIS

Accepted Article

Title: Key-lock ceria catalysts for the control of diesel engine soot particulate emissions

Authors: Débora Sorolla-Rosario, Esther Bailón-García, Arantxa Davó-Quiñonero, Dolores Lozano-Castelló, and Agustín Bueno-López

To be cited as: *ChemCatChem* 10.1002/cctc.201902177

Link to VoR: http://dx.doi.org/10.1002/cctc.201902177

A Journal of
ChemPubSoc Europe

WILEY-VCH

www.chemcatchem.org

10.1002/cctc.201902177

WILEY-VCH

FULL PAPER

Key-lock ceria catalysts for the control of diesel engine soot particulate emissions

Débora Sorolla-Rosario, Arantxa Davó-Quiñonero, Esther Bailón-García*, Dolores Lozano-Castelló, Agustín Bueno-López

D. Sorolla-Rosario, Dr. Arantxa Davó-Quiñonero, Dr. Esther Bailón-García*, Prof. Dolores Lozano-Castelló, Prof. Agustín Bueno-López
Department of Inorganic Chemistry
University of Alicante
Carretera de San Vicente s/n, E03080, Alicante, Spain
E-mail: estherbg@ugr.es

Supporting information for this article is given via a link at the end of the document

Abstract: A new concept, referred to as key-lock catalyst, is presented in this article. Soot combustion ceria catalysts were prepared combining hard (polymethylmethacrylate colloidal crystals) and soft (Pluronic F127) templates, tuning the porosity of ceria in different size ranges to match the morphology of soot aggregates. The catalysts porosity was characterized in detail by N_2 adsorption-desorption isotherms and Hg-porosimetry. XRD and H_2-TPR characterization ruled out that differences in activity are related neither with crystallographic nor with redox properties. As a proof of key-lock catalyst concept, an optimum key-lock ceria catalyst was synthesized by combining large macropores (100-300 nm) with mesopores (10-30 nm), because they fit to the large soot aggregates and to primary soot particles sizes, respectively. The best soot combustion activity of the optimum key-lock catalyst is attributed to the optimum transfer of ceria active oxygen from catalyst to soot. The catalytic results confirmed that all ceria catalysts prepared with different porosity oxidize NO to NO_2 at the same rate, and the NO_2-assisted soot combustion pathway is not affected by tuning ceria porosity. This double-templated synthesis and the key-lock concept opens a new synthesis approach to design noble-metal free soot combustion catalysts based on the highly effective active oxygen mechanism.

Introduction

The most harmful pollutants generated in diesel engines are CO, HC, NO_x, and particulate matter (soot),[1] from which, soot is the second pollutant with the highest proportion in pollutant emissions.[2] Particle filters are employed to retain soot particles from the diesel exhaust, nevertheless, oxidative regeneration of these filters is required to eliminate the accumulated soot.[3]
The soot oxidation using the NO_x and O_2 present in the exhaust is the easiest way to regenerate the filters, nevertheless the temperature required for the rapid and spontaneous oxidation of soot in air (500-600 ºC)[4] is not reached in typical work cycles (150-450 ºC).[3,5] Thus, a catalyst must to be placed on the particle filter to decrease the ignition temperature of soot.

CeO_2 is one of the most studied soot combustion catalyst because of its capacity to store and release highly oxidizing oxygen species, and different foreign cations, such as Zr, La or Pr,[6–9] have been loaded into the ceria lattice to enhance its catalytic features.[10] These dopants improve the thermal stability, oxygen storage capacity, surface reducibility, oxygen mobility within the framework, etc.[11]

Two main reaction mechanisms have been proposed to accelerate soot combustion in diesel exhaust conditions.[11–13] One of them is the so-called NO_2-assisted mechanism, in which the role of the catalyst is to accelerate the NO to NO_2 oxidation, being NO_2 the most oxidizing specie in the gas mixture.[14] The other one is the active-oxygen mechanism, where a catalyst like ceria exchanges oxygen atoms with the gas phase molecules (mainly with O_2 and NO_2) and the active oxygen radicals yielded upon the exchange carry out soot oxidation. Nonetheless, in a scenario with low NO_x emissions by the new generation of diesel engines, the active oxygen mechanism plays the determinant role in the combustion of soot. Nonetheless, in this case, the activity of soot combustion catalysts is limited by the active oxygen transfer from the catalysts to the soot and thus, the soot-catalyst contact. Consequently, the optimization of such contact must be kept in mind together with the improvement of the physicochemical and catalytic properties of ceria.[15] The catalyst morphology plays an crucial role in solid-solid catalytic reactions in which the number of contact points is essential to ensure the course of the reaction. In that sense, different engineered morphologies have been analyzed to improves soot-catalyst contact.[16,17] P. Miceli et al.[18] have investigated the influence of three ceria morphologies in the soot oxidation: uncontrolled, nanofibers and self-assembled stars. Ceria nanofibers presents the lowest surface area (4 m^2/g), however their catalytic activity in soot combustion is better than unstructured ceria (31 m^2/g) because these nanofibers can be arranged as a network inside the channels of the particulate filter favoring the trapping of soot particles via several contact points. In the case of the ceria stars, both the specific surface area (105 m^2/g) and number of points of contact were enhanced and consequently, an improved catalytic activity was obtained regarding other morphologies. A. Trovarelli et al.[19] have demonstrated that more exposed surfaces improves the soot oxidation and thus, an increase in activity was obtained with nano-shaped materials regarding conventional ceria. W. Zhang et al.[20] prepared ceria nanorod, nanoparticle and flake via hydrothermal and solvothermal methods and tested them in soot combustion observing that CeO_2 nanorod display the best activity for the soot combustion. J. Llorca et al.[21,22] have also demonstrated the redox behavior and soot oxidation potential of ceria-based catalysts when suitable carbon-catalyst arrangements are generated at nanoscale. They show that the building of an appropriate interface at nanoscale can result in unexpected chemical functionalities.
Considering the same concept, three-dimensionally ordered macroporous (3DOM) catalysts have demonstrated an improved activity in soot combustion in comparison to their disordered equivalent, which was associated to the enhanced soot-catalyst contact.[23–25] However, this porosity is not optimized to the soot morphology and only several contact points are still achieved.

3DOM structures are composed by spherical voids typically with 50-300 nm of diameter[26–29] whereas soot particles are formed by agglomerated spherical primary particles with an average primary particles diameter ranging from 10 to 25 nm and average aggregate sizes in the range of 50 to 300 nm.[30–33] Thus, despite spherical voids of 3DOM structures have similar sizes to soot particles, soot are not spherical particles but are formed by agglomerates of few-nanometer particles and consequently, only touch the smooth 3DOM surface in several points.

In order to optimize the 3DOM structure, in this manuscript hierarchical 3DOM cerias were synthesized and their catalytic behaviour as soot combustion catalyst was studied and deeply analysed based on their chemical and porous texture. The porosity of ceria catalysts has been tuned and optimised to match the morphology of the soot aggregates, therefore maximizing the transfer of active oxygen between both types of complex solid particles. This novel concept presented in this article is referred to as key-lock catalyst. Key-lock ceria catalysts have been prepared combining hard (polymethylmethacrylate colloidal crystals, PMMA) and soft (Pluronic F127) templates, tuning the porosity of ceria in different size ranges to match the morphology of soot aggregates. CeO_2 catalysts without 3DOM structured morphology (named as "Ref") have been also synthesized and studied for comparisons purposes.

Results and Discussion

Morphology of key-lock catalysts

The morphology of samples was analyzed by FESEM and representative images are shown in **Figure 1**. Both reference samples present a closed structure in comparison with 3DOM samples, and differences are observed if F127 is added. A closed surface with several fissures is observed in the reference sample prepared without F127 whereas a rough surface is identified when F127 is added, which could be indicative of the creation of new porosity by the soft-template process. On the contrary, a compact three-dimensionally ordered macroporous (3DOM) structure is observed in samples prepared using the PMMA hard template both without (0-3DOM) and with low amount of surfactant (0.8-3DOM). This 3DOM structure is the negative of the PMMA hard template, as observed in the FESEM image of the PMMA colloidal crystal. The 3DOM structure is disrupted and opened in samples prepared with medium concentration of surfactant (2.7 and 7.9 mM) in which voids of the order of few hundred of nanometers are observed. This disruption of the 3DOM structure is more significant in samples prepared with a F127 concentration of 7.9 mM, but the 3DOM structure is still observed. At very high concentration of surfactant, the 3DOM structure is practically not observed and a closed surface with several fissures is shown. In these cases, most of the cerium precursor cannot enter within the PMMA interstices and thus, an agglomeration of ceria particles is observed.

Textural properties of key-lock catalysts

N_2 adsorption-desorption isotherms are depicted in **Figure 2a**, and data calculated from these isotherms are collected in **Table S1**. All catalysts show a type II isotherm according to the IUPAC classification, characteristics of non-porous or macroporous adsorbents. The 0-Ref sample shows low N_2 adsorption in comparison with PMMA-templated samples, and the addition of F127 clearly affects the porous texture of the Ref sample (compare 0-Ref with 7.9-Ref). Higher adsorption of N_2 is observed along with a better defined H_2 hysteresis loop for 7.9-Ref, which manifest the creation of porosity by the soft-template action of F127 (S_{BET} and V_{meso} increases, **Table S1**) corroborating the observation obtained from SEM images.

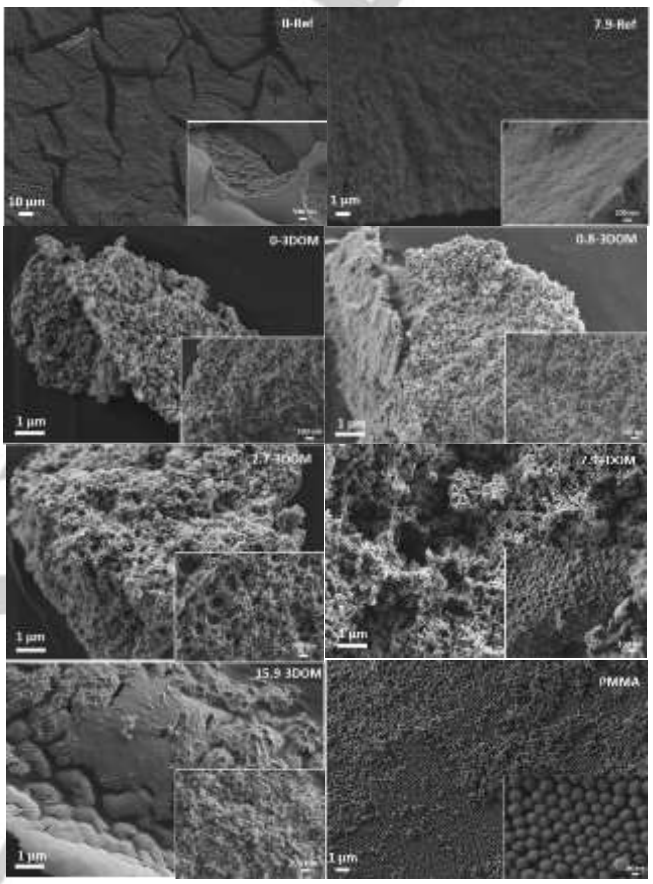

Figure 1. FESEM images of Ref and 3DOM catalysts, and of the PMMA hard template.

All PMMA-templated samples present similar and low N_2-adsorption at low relative pressures, denoting low micropores volume (**Table S1**). Nonetheless, a well-defined H_3 hysteresis loop appears at high relative pressures (P/P_0 range of 0.8-1) for the 0-3DOM sample, which is characterized by a rapid increase of the slope at relative pressures close to 1 due to the presence of macropores. This hysteresis loop is clearly influenced by the concentration of F127 used in the synthesis. Increasing the amount of F127, the H_3 hysteresis loop decreases until almost disappear at concentration higher than 7.9 mM, denoting reduction of the macropores volume. In addition, in presence of high concentration of surfactant, a H_2 hysteresis loop appears at lower relative pressure (P/P_0 range of 0.4–0.8) demonstrating the formation of mesopores. Note also that the higher is the F127 concentration, the lower is the relative pressures in which the hysteresis loop close. This fact manifests a narrowing of the mesopores width by increasing the amount of F127.

To corroborate this fact, BJH method was applied to the N_2-isotherms desorption branch (**Figure 2b**). Two different regions are identified in the pore size distributions: narrow mesopores of

3.5-5 nm and wide mesopores ranging from 12 to 32 nm. These regions are clearly affected by the presence and concentration of the soft template F127 and the hard template PMMA. Ceria Ref (0-Ref) sample presents a very low amount of mesopores with 3.2 nm. The addition of F127 (7.9-Ref) creates mesopores with uniform pore size of 5 nm of diameter. Ceria-3DOM sample prepared without F127 (0-3DOM) presents mesopores of around 32 nm and narrow mesopores are not detected. The addition of F127 in the synthesis creates new mesoporosity of 3.5 nm and causes a narrowing (**Figure 2c**) and a decrease of the widest mesoporosity. The higher is the concentration of F127, the higher is the volume of mesopores of 3.5 nm as well as the narrowing and the decrease of the widest porosity. This could indicate that the former (3.5 nm) is new mesoporosity created by the addition of F127 whereas the latter (12-32 nm) is existing mesoporosity created by the formation of the 3DOM structure which is affected in some way by the addition of F127.

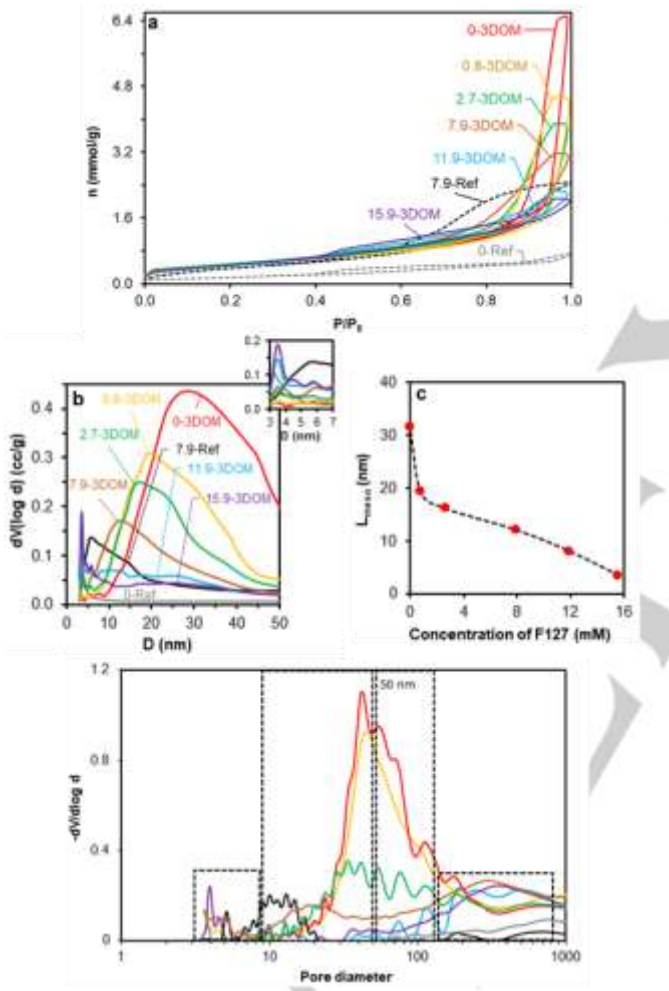

Figure 2. a) N_2 Adsorption-Desorption isotherms, b) BJH distribution of hierarchical 3DOM and Ref CeO_2-catalysts, c) relationship between mesopore width (L_{meso}) and concentration of Pluronic F127 used in the synthesis and d) Hg-porosimetry of hierarchical 3DOM and Ref ceria catalysts.

Hg-porosimetry characterization was performed in order to well characterize the meso and macroporosity of samples, and results are collected in **Figure 2d** and **Table S1**. Here, four different regions are observed. According to BJH, two type of pores are observed in the mesoporosity range at different sizes: 3.5-5 nm and 10-50 nm. As commented above, the narrow mesopores volume increases and the pore width and pore volume of the widest mesoporosity decrease by increasing the amount of F127. Regarding the macroporosity range observed in Hg-porosimetry characterization (**Figure 2d**), a peak is observed at 60-70 nm ascribed to spherical voids created by the PMMA combustion. This peak decreases by increasing the concentration of F127 until almost disappear at F127 concentration higher than 2.7 mM, but appearing a new peak at around 300 nm. These observations are corroborated by the analysis of the pore volume distributions (**Table S1**). It is observed that the narrow mesoporosity ($V_{3.5\text{-}10}$) increases with the addition of increasing amounts of F127, whereas the wide mesoporosity ($V_{10\text{-}50}$) and narrow macroporosity ($V_{50\text{-}150}$) decreases by increasing the concentration of F127. In addition, wide macroporosity increases up to achieve an optimum at a concentration of 7.9 mM. In other words, despite new mesoporosity is created by the addition of F127, the existing mesoporosity and macroporosity is reduced and thus, S_{BET} is constant. It is important to highlight that a pore distribution with two clear regions is obtained for a concentration of 7.9 mM with mesopores of 10-30 nm and macropores of 100-500 nm and consequently, it could be said that a reordering of the porosity occurs adding F127. Note that this two-ranged porosity is adapted to the soot morphology, consisting of aggregates ranging from 50 to 300 nm of spherical primary particles with an average diameter of 10-25 nm, and as it is demonstrated afterwards, this proper match between the shapes of soot and catalyst is very positive for the catalytic combustion. This match between soot and catalyst shapes is defined in this article as key-lock catalyst.

To explain these textural and morphological changes with the concentration of F127, morphological characteristics of ceria 3DOM structures and properties of pluronic F127, such as the critical micelle concentration (cmc) and the average micelle size in ethanol, must to be taken into account. Regarding 3DOM structures, a bimodal pore size distribution was described in the 3DOM-ceria catalysts;[34] corresponding to the interstitial spaces generated between the PMMA spheres that have not been completely filled by the precursor solution during the infiltration and to the porosity obtained by calcination of PMMA spheres. With respect to the properties of F127, the cmc of F127 in pure ethanol was estimated in 2.6 mM from literature data.[35] The cmc of P127 was measured in different mixtures of ethanol-water and thus, the cmc in pure ethanol was estimated by extrapolation to a concentration of 100 % ethanol (**Figure S1**). In turn, the average size of F127 micelle obtained by real and simulated experiences was 20-25 nm.[36,37] It is well known that the introduction of F127 to the CeO_2 wall generates mesopores ranging from 2 to 5 nm.[38,39]

With these considerations, a plausible mechanism of the effect of F127 on the morphological and textural properties has been proposed. In **Figure 3** a graphical mechanism is depicted.

In the sample prepared without F127 (0-3DOM), a bimodal pore size distribution is obtained (BJH and Hg-Porosimetry). The ethanolic solution of cerium citrate is infiltrated inside the voids between PMMA spheres but after drying the cerium citrates are concentrated around the PMMA particles generating interstitials voids of around 32 nm after calcination of PMMA spheres, which also generates the macroporous structure (pores of 60 nm).

The addition of F127 has drastic effects depending on its concentration. At low concentration (0.8-3DOM), surfactant molecules are dispersed into the ethanolic solution of cerium

citrate without forming micelles, and are infiltrated without problems into the PMMA interparticle voids. With the gradual removal of solvent upon drying, the concentration of F127 rises to a value higher than the critical micelle concentration[39] and thus, micelles are formed which increases the thickness of the cerium citrate layer. This increase of thickness causes a decrease of the interstitial pores size up to 24 nm and the presence of micelles inside cerium citrate layer creates a certain mesopores volume of 3.5 nm after the calcination step.

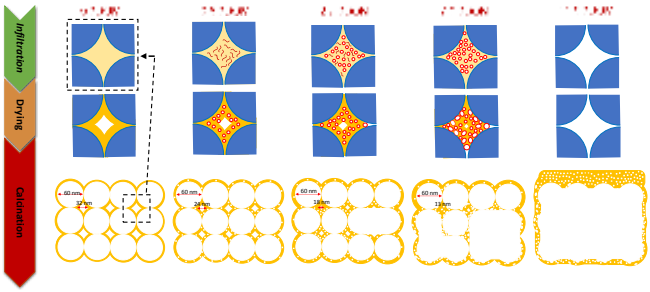

Figure 3. Textural modification by the addition of different concentration of pluronic F127 to the ceria precursor solution for the synthesis of CeO_2 3DOM.

Increasing the F127 concentration to 2.7 mM (2.7-3DOM), the critical micelle concentration is achieved and thus, part of the surfactant molecules is forming micelle before the infiltration. Again, after the infiltration, the thickness of the cerium citrate layer increases in more proportion and the interstitial pore size decreased (18 nm). However, part of the micelles created before infiltration could block the ultrathin spaces between two neighbouring PMMA spheres and be inaccessible to the cerium citrate solution, disrupting the 3DOM structure and creating macropores of higher size.

This effect is more pronounced at a concentration of 7.9 mM. In this case most of the surfactant molecules are forming micelles prior to the infiltration and after drying these micelles can even coalesce and grow with the gradual removal of the solvent due to the high amount of surfactant and the low solution volume. This causes again a decrease of the interstitial size together with a partial block of the PMMA interparticle connection channels causing a more significant disruption of the 3DOM structure. At this point a perfectly defined bimodal pore size distribution is obtained with mesopores of 10-30 nm and macropores of 100-500 nm (**Figure 2d**). Above 7.9 mM (11.9 or 15.9 mM), the concentration is high enough to produce a micelle coalescence previous to the infiltration and consequently, the infiltration is hampered and thus, 3DOM structure is not formed.

Crystalline structure (XRD), reducibility (H_2-TPR) and Raman spectroscopy.

H_2-TPR was used to study the reducibility of catalysts and results are shown in **Figure 4a**. The H_2-TPR profiles present two peaks of reducibility localized at around 580 ºC and 780 ºC that can be ascribed to the reduction of Ce^{4+} cations in the ceria surface and into the bulk ceria, respectively. Note that the reduction of ceria surface is improved in PMMA-templated samples regarding Ref ones, which has been attributed to the O_2-poor environment created during PMMA combustion.[23] However, no significant differences are observed in the profiles of the analysed 3DOM samples denoting a similar reducibility. Consequently, it could be said that the use of F127 in the CeO_2-3DOM synthesis does not affect the reducibility of the ceria. Raman spectra were also recorded to analyze the effect of template in the oxygen vacancies generation (**Figure 4b**). Note that similar spectra were obtained in all cases manifesting that F127 neither affects the oxygen vacancies generation nor the vibration of the oxygen sub-lattice.

XRD was analyzed in order to characterize the crystalline structure of the catalysts. **Figure 4c** shows the X-Ray diffractograms. The positions of XRD lines for all catalysts were the same and correspond to the standard CeO_2 XRD pattern (JCPDS PDF no. 34-0394) ascribed to a face-centred cubic crystal structure. The intensity of the peaks decreases and the full-width at half-maximum (FWHM) increases by increasing the F127 concentration, denoting an inhibition of the growth of metal oxide particles by the presence of F127 (**Figure 4d**). This suggests that the presence of surfactant molecules together with the metal salt upon solvent evaporation inhibit the growth of metal oxide particles during calcination, and stabilize a crystal size of 13 nm at high concentration of F127 (> 2.65 mM).[39]

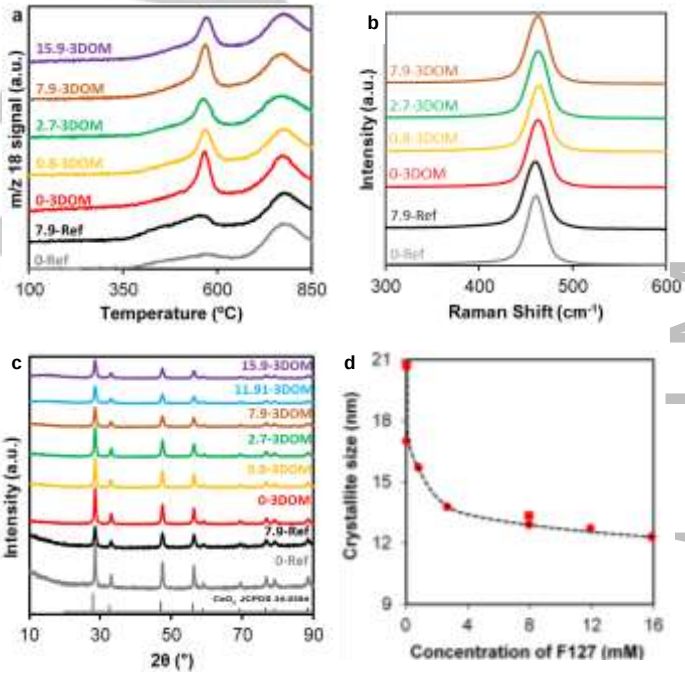

Figure 4. a) H_2-TPR results, b) Raman spectra of the catalysts and c) XRD pattern of 3DOM and Ref CeO_2-samples. d) relationship between crystallite size and concentration of Pluronic F127 used in the synthesis (cycles: 3DOM catalysts; squares: Ref catalysts).

Catalytic performance of key-lock catalysts in the soot combustion

Soot combustion experiments were performed under a $NO_x/O_2/N_2$ gas mixture. In this case, two mechanism are involved in the soot combustion reaction: the active oxygen and the NO_2-assisted mechanisms. The chemical nature and the reducibility of all samples are quite similar, and therefore, no significant differences in the ability to oxidase NO to NO_2 could be expected. In order to identify the NO oxidation ability of samples and NO_2 reactivity, NO oxidation to NO_2 catalytic experiments were performed without and with soot (**Figure 5**). Similar profiles are obtained both in presence and absence of soot for all catalysts,

which denotes similar oxidation of NO to NO_2 and similar NO_2 consumption by soot reaction. Thus, the different catalytic performance of the catalysts can only be related with the different textural properties.

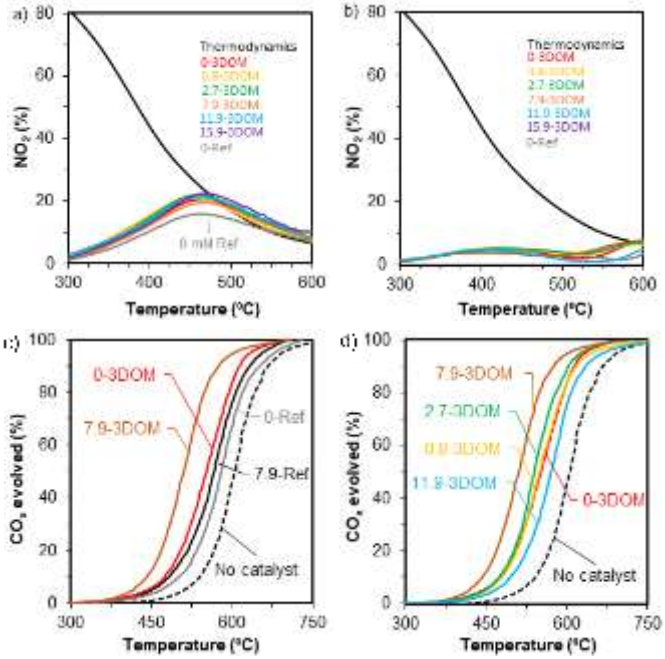

Figure 5. NO oxidation to NO_2 in catalytic experiments performed (a) without soot and (b) with soot and soot combustion experiments of (c) 3DOM and Ref samples and (d) hierarchical CeO_2-3DOM catalysts. Conditions: 500 ppm NO_x + 5% O_2 + N_2.

The soot combustion catalytic behaviour of samples was analysed by the CO_x evolved during the catalytic tests, and results are depicted in **Figure 5c** and **d**. All catalysts accelerate the combustion of soot regarding the uncatalyzed reaction. However, the catalytic activity depends on the catalyst morphological and textural properties. Both the 3DOM structure and the F127-template action clearly affect the catalytic activity (**Figure 5c**). The 3DOM structure improves the soot-catalyst contact, improving the combustion activity with respect to Ref catalysts. However, this improvement is more significant in F127-templated samples (7.9-3DOM vs 7.9-Ref), which indicates that the F127-template action is different depending on the morphological structure. As was pointed out previously, the addition of F127 (7.9-Ref) during the synthesis of CeO_2 reference material (0-Ref) increase the surface area of the sample (**Table S1**) due to the generation of mesoporosity of around 5.5 nm (**Figure 2** and **Table S1**), which improves the soot-catalyst contact. However, this improvement occurs only on the external surface because of the large size of soot aggregates (50-300 nm). In the case of 3DOM samples, the addition of F127 (7.9-3DOM), not only creates new porosity but also produce a reordering of the porosity being adapted to the soot morphology. At low concentration of F127 (0.8-3DOM), mesoporosity of around 3.5 nm is created but the 3DOM structure is not disrupted and the activity is similar to the 0-DOM sample (**Figure 6b**). Increasing the concentration above the critical micelle concentration, the 3DOM structure is disrupted by the addition of F127 creating, at 7.9 mM concentration, an optimal bimodal pore distribution of large macropores (100-300 nm) and narrow mesopores (10-30 nm). Thus, an optimum porosity is created being adapted to the soot morphology, which significantly increases the soot-catalyst contact and, consequently, the catalytic activity (**Figure 6b**). This is referred to as key-lock contact, which is depicted in **Figure 6a**.

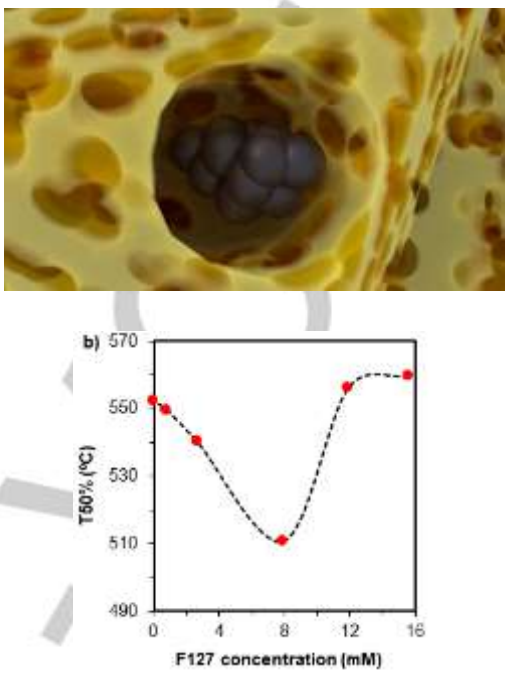

Figure 6. a) Schematic representation of soot-catalysts optimized contact in 7.9-3DOM sample and b) T50% with respect to F127 concentration for hierarchical CeO_2-3DOM catalysts.

Above 7.9 mM of F127 concentration, the formation of the 3DOM structure is hindered and the catalytic activity decreases, the catalytic behaviour being comparable with that obtained using Ref catalysts.

As it is observed in **Figure 6b**, the optimum key-lock soot-catalyst contact is achieved with the 7.9-3DOM catalyst. As demonstrated in previous characterization, all 3DOM catalysts have similar redox properties and are able to oxidise NO to NO_2 at the same rate. This suggests that the contribution of the NO_2-assited mechanism to soot combustion is similar in all cases, and differences in the production of active oxygen species are neither expected. Therefore, the best behaviour of the optimum key-lock catalyst is the improved transfer of active oxygen from catalyst to soot.

Recent research in the development of soot combustion metal oxide catalysts is mainly focussed on two ways: the maximum production of active oxygen and the improvement of the active oxygen transfer from catalyst to soot. This article demonstrates that tuning the porosity of the catalyst combining both soft and hard templates is possible to match the shape of soot primary particles and aggregates, obtaining a key-lock interaction that maximizes the contact, and therefore, the transfer of active oxygen.

Conclusion and outlook

Soot combustion ceria catalysts have been prepared combining hard (PMMA colloidal crystals) and soft (Pluronic F127) templates, tuning the porosity of ceria in different size ranges to match the morphology of soot aggregates.

The PMMA hard template generates a bimodal pore size distribution in ceria, combining interstitials voids of around 32 nm and pores of 60 nm due to PMMA spheres removal.

The additional utilization of the soft template F127 has two effects in the porosity of 3DOM Ceria. On the one hand, the soft template combustion generates mesopores of 3.5 nm, and on the other hand, the infiltration of the cerium precursor together with F127 into the PMMA template affects the interstitial mesopores created into the hard template. These effects of F127 depend on the F127 concentration, and the higher the concentration the higher the amount of mesopores with 3.5 size, but also the lower the size of the mesopores created into the PMMA interstices and the larger the pores created upon PMMA removal.

As a proof of key-lock catalyst concept, an optimum key-lock ceria catalyst has been synthesised combining large macropores (100-300 nm) with mesopores (10-30 nm), because they fit to the large soot aggregates and to the primary soot particles size, respectively. It has been demonstrated that, the best soot combustion activity of the optimum key-lock ceria catalyst is attributed to the optimum transfer of ceria active oxygen from catalyst to soot. XRD and temperature programmed reduction with H_2 characterization ruled out that differences in activity are related neither with crystallographic nor with redox properties.

The catalytic results confirmed that, all ceria catalysts prepared with different porosity oxidise NO to NO_2 at the same rate, and the NO_2-assisted soot combustion pathway is not affected by tuning ceria porosity.

The double-templated synthesis and the key-lock concept presented in this study opens a new synthesis approach to design noble-metal free soot combustion catalysts based on the highly effective active oxygen mechanism. Once optimized the soot-catalyst contact with the new key-lock catalysts to maximize the active oxygen transfer from catalyst to soot, modification of the chemical properties of ceria could be performed in order to maximize the production of active oxygen. At this way, advanced catalysts could be designed combining a superior generation and transfer of active oxygen which overcome the catalytic performance of expensive noble metal-based soot catalysts

Overall, we believe that the present work provides a remarkable contribution towards the implementation of these key-lock catalysts for the abatement of diesel engines particles emissions, which are technologies for pollution prevention.

Experimental Section

Synthesis of key-lock catalysts. CeO_2-3DOM catalysts were prepared using polymethylmethacrylate (PMMA) colloidal crystals as hard template. PMMA colloidal crystals were prepared following the methodology previously described elsewhere.[23,24] After synthesis, a cerium citrate ethanolic solution was infiltrated into the PMMA colloidal crystals. This cerium citrate solution (0.476 M) was obtained by dissolving cerium nitrate ($Ce(NO_3)_3{\cdot}6H_2O$) and citric acid in stoichiometric proportion in ethanol. Then, the infiltrated solid was finally calcined to remove the PMMA template for 6 h at 600 °C (1 °C/min).

Several CeO_2-3DOM catalysts with hierarchical porosity were synthesized using the described method but modified in some cases including additionally a soft template. For that, the proper amount of triblock surfactant Pluronic F127 was dissolved in the ethanolic solution of cerium precursor. The surfactant concentration in this solution was ranged from 0 to 15.9 mM. These solutions were infiltered in the PMMA colloidal hard template and calcined, as described above. Catalysts were referred to as X-3DOM (X corresponding to the concentration of surfactant F127 used, e.g. 7.9-3DOM catalyst was prepared using a concentration of F127 of 7.9 mM). Reference materials (X-Ref) were also prepared by direct calcination of the dried ethanolic solution of citric acid, F127 and the cerium nitrate.

Characterization of key-lock Catalysts. Morphology of catalysts was studied by Field Emission Scanning Electron Microscopy in a Merlin VP Compact FESEM microscope from Zeiss. N_2 adsorption, mercury intrusion porosimetry and Helium density analysis were performed to characterize the catalysts textural properties. N_2 adsorption-desorption isotherms were performed at -196 °C using an Autosorb-6 equipment from Quantachrome. Previously to the adsorption tests, the catalysts were outgassed at 150 °C for 2 h under vacuum. The Brunauer, Emmett and Teller (BET) equation and the Barrett, Joyner and Halenda (BJH) method were used to determine the apparent surface area (S_{BET}) and the mesopore volume (V_{mes}) and mesopore width (L_{meso}), respectively. The catalysts macroporosity and the closed porosity were studied by Hg-porosimetry and He-pycnometry, respectively, using a Poremaster 60 GT and a MicroUltrapyc 1200e automatic He-pycnometer from Quantachrome in each case.

The crystallinity and reducibility of catalysts were determined by X-ray diffraction and Temperature Programmed Reduction experiments with H_2 (H_2-TPR), respectively. Diffractograms were registered in a 2θ range from 10 to 90° with a step of 0.025° using a Rigaku Miniflex II diffractometer with CuKα radiation (λ=0.15418 nm). The crystal size (D) was determined using the Scherrer's equation. H_2-TPR experiments were performed using a TGA/SDTA851 thermobalance from Mettler Toledo coupled to a Thermostar GSD301 T mass spectrometer from Pfeiffer Vacuum. For that, 20 mg of catalyst were heated at 10 °C/min under H_2 flow (40 ml/ min of a mixture of 5% H_2 in Ar) up to 900 °C.

Chemical characterization was performed by X-ray photoelectron spectroscopy (XPS) using a K-ALPHA Thermo Scientific device equipped with Al-Kα radiation (1486.6 eV). C1s transition at 284.6 eV was used as internal reference to adjust the binding energy scale.

A dispersive Raman Jasco NRS-5100 Spectrometer with a He-Ne laser source (632.8 nm) was used for Raman spectroscopy characterization. 2 scans obtained with 1.8mW laser power were averaged to obtain each spectrum.

Catalytic tests. Catalytic tests were carried out at programmed temperature from room temperature to 700 ºC with a heating rate of 10 °C/min using a fixed-bed tubular quartz reactor. For that, 20 mg of carbon black (Printex U), 80 mg of catalyst and 300 mg of SiC were mixed with a spatula in the so-called loose-contact mode in order to obtain results with practical meaning. The gas mixture used (500 ml/min; GHSV=30,000 h^{-1}) was composed of 500 ppm NO and 5% O_2 in N_2. The exhaust gases composition was analyzed in Specific NDIR-UV gas analyzers (BINOS 100, 1001 and 1004) for CO, CO_2, NO, NO_2 and O_2 from Fisher–Rosemount.

Acknowledgements

The authors thank the financial support of the Spanish Ministry of Economy and Competitiveness (Project CTQ2015-67597-C2-2-R and grant FJCI-2015-23769), the Spanish Ministry of Education, Culture and Sports (grant FPU14/01178), Generalitat Valenciana (Project PROMETEO/2018/076 and APOSTD/2019/030), the Spanish Society of Catalysis (SECAT-"initiation for research in catalysis") and the UE (FEDER funding). Authors also thank the graphical support provided by Daniel D. Paredes Martínez.

Keywords: Key–lock catalysts • soot • diesel • 3DOM • ceria

[1] J. P. A. Neeft, M. Makkee, J. A. Moulijn, *Fuel Process. Technol.* **1996**, *47*, 1.

[2] I. A. Reşitołlu, K. Altinişik, A. Keskin, *Clean Technol. Environ. Policy* **2015**, *17*, 15.

[3] A. Yezerets, N. W. Currier, H. K. Do, H. A. Eadler, W. S. Epling, C. H. F. Peden, *Appl. Catal. B Environ.* **2005**, *61*, 120.

[4] N. Russo, D. Fino, G. Saracco, V. Specchia, *J. Catal.* **2005**, *229*, 459.

[5] M. V. Twigg, *Appl. Catal. B Environ.* **2007**, *70*, 2.

[6] V. Rico-Pérez, E. Aneggi, A. Bueno-López, A. Trovarelli, *Appl. Catal. B Environ.* **2016**, *197*, 95.

[7] M. Piumetti, S. Bensaid, N. Russo, D. Fino, *Appl. Catal. B Environ.* **2016**, *180*, 271.

[8] D. Mukherjee, B. G. Rao, B. M. Reddy, *Appl. Catal. B Environ.* **2016**, *197*, 105.

[9] L. Soler, A. Casanovas, C. Escudero, V. Pérez-Dieste, E. Aneggi, A. Trovarelli, J. Llorca, *ChemCatChem* **2016**, *8*, 1.

[10] D. Jampaiah, V. K. Velisoju, D. Devaiah, M. Singh, E. L. H. Mayes, V. E. Coyle, B. M. Reddy, V. Bansal, S. K. Bhargava, *Appl. Surf. Sci.* **2019**, *473*, 209.

[11] H. Zhu, J. Xu, Y. Yichuan, Z. Wang, Y. Gao, W. Liu, H. Yin, *J. Colloid Interface Sci.* **2017**, *508*, 1.

[12] W. F. Shangguan, Y. Teraoka, S. Kagawa, *Appl. Catal. B Environ.* **1997**, *12*, 237.

[13] A. Bueno-López, *Appl. Catal. B Environ.* **2014**, *146*, 1.

[14] A. Setiabudi, B. A. A. L. Van Setten, M. Makkee, J. A. Moulijn, *Appl. Catal. B Environ.* **2002**, *35*, 159.

[15] S. Wu, Y. Yang, C. Lu, Y. Ma, S. Yuan, G. Qian, *Eur. J. Inorg. Chem.* **2018**, *2018*, 2944.

[16] S. Liu, X. Wu, W. Liu, W. Chen, R. Ran, M. Li, D. Weng, *J. Catal.* **2016**, *337*, 188.

[17] E. Sartoretti, C. Novara, F. Giorgis, M. Piumetti, S. Bensaid, N. Russo, D. Fino, *Sci. Rep.* **2019**, *9*, 9.

[18] P. Miceli, S. Bensaid, N. Russo, D. Fino, *Nanoscale Res. Lett.* **2014**, *9*, 1.

[19] E. Aneggi, D. Wiater, C. De Leitenburg, J. Llorca, A. Trovarelli, *ACS Catal.* **2014**, *4*, 172.

[20] W. Zhang, X. Niu, L. Chen, F. Yuan, Y. Zhu, *Nat. Publ. Gr.* **2016**, 1.

[21] M. Aouine, E. Aneggi, J. Llorca, A. Trovarelli, P. Vernoux, *Chem. Commun.* **2019**, *55*, 3876.

[22] E. Aneggi, V. Rico-perez, C. De Leitenburg, S. Maschio, L. Soler, J. Llorca, A. Trovarelli, *Angew. Chemie* **2015**, *127*, 14246.

[23] V. Alcalde-Santiago, E. Bailón-García, A. Davó-Quiñonero, D. Lozano-Castelló, A. Bueno-López, *Appl. Catal. B Environ.* **2018**, *In press*, 6.

[24] V. Alcalde-Santiago, A. Davó-Quiñonero, D. Lozano-Castelló, A. Bueno-López, *Appl. Catal. B Environ.* **2018**, *234*, 187.

[25] A. A. Voskanyan, K. Y. Chan, C. Y. V. Li, *Chem. Mater.* **2016**, *28*, 2768.

[26] N. Feng, Y. Wu, J. Meng, C. Chen, L. Wang, H. Wan, G. Guan, *RSC Adv.* **2015**, *5*, 91609.

[27] Y. Wei, Z. Zhao, X. Yu, B. Jin, J. Liu, C. Xu, A. Duan, G. Jiang, S. Ma, *Catal. Sci. Technol.* **2013**, *3*, 2958.

[28] Y. Wei, J. Liu, Z. Zhao, A. Duan, G. Jiang, *J. Catal.* **2012**, *287*, 13.

[29] G. Zhang, Z. Zhao, J. Xu, J. Zheng, J. Liu, G. Jiang, A. Duan, H. He, *Appl. Catal. B Environ.* **2011**, *107*, 302.

[30] S. China, G. Kulkarni, B. V. Scarnato, N. Sharma, M. Pekour, J. E. Shilling, J. Wilson, A. Zelenyuk, D. Chand, S. Liu, A. C. Aiken, M. K. Dubey, A. Laskin, R. A. Zaveri, C. Mazzoleni, *Environ. Res. Lett.* **2015**, *10*, 114010.

[31] Y. Ma, M. Zhu, D. Zhang, *Appl. Energy* **2014**, *113*, 751.

[32] J. O. Müller, D. S. Su, U. Wild, R. Schlögl, *Phys. Chem. Chem. Phys.* **2007**, *9*, 4018.

[33] B. A. A. L. Van Setten, M. Makkee, J. A. Moulijn, *Catal. Rev. - Sci. Eng.* **2001**, *43*, 489.

[34] A. Davó-Quiñonero, J. González-Mira, I. Such-Basañez, J. Juan-Juan, D. Lozano-Castelló, A. Bueno-López, *Catalysts* **2017**, *7*, 67.

[35] B. Sarkar, V. Ravi, P. Alexandridis, *J. Colloid Interface Sci.* **2013**, *390*, 137.

[36] X. Meng, J. Liu, X. Yu, J. Li, X. Lu, T. Shen, *Sci. Rep.* **2017**, *7*, 1.

[37] D. Bedrov, C. Ayyagari, G. D. Smith, *J. Chem. Theory Comput.* **2006**, *2*, 598.

[38] H. Zhang, L. Zhang, J. Deng, Y. Liu, H. Jiang, F. SHI, K. Ji, H. Dai, *Chinese J. Catal.* **2011**, *32*, 842.

[39] H. Li, L. Zhang, H. Dai, H. He, *Inorg. Chem.* **2009**, *48*, 4421.

10.1002/cctc.201902177

Key-lock ceria catalysts for the control of diesel engine soot particulate emissions

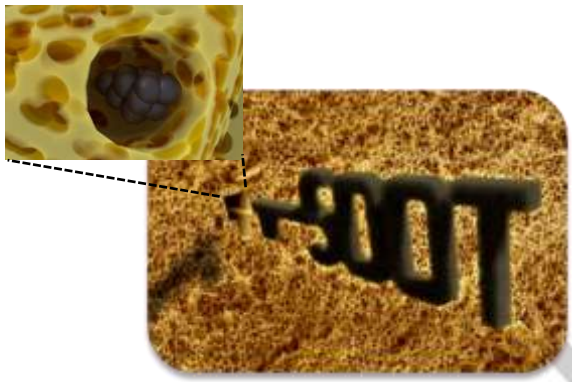

The porosity of the ceria catalysts was tuned combining hard and soft templates to match the morphology of soot aggregates. An optimum key-lock ceria catalyst was synthesized by combining large macropores (100-300 nm) with mesopores (10-30 nm), because they fit to the large soot aggregates and to primary soot particles sizes obtaining a superior catalytic performance for soot combustion.

Supporting Information

Key-lock ceria catalysts for the control of diesel engine soot particulate emissions

Débora Sorolla-Rosario, Arantxa Davó-Quiñonero, Esther Bailón-García, Dolores Lozano-Castelló, Agustín Bueno-López*

Table S1. Textural properties of ceria catalysts

	N_2-isotherms				Hg-Porosimetry				
Sample	S_{BET} (m^2/g)	V_{mic}* (cm^3/g)	V_{meso}* (cm^3/g)	L_{meso} (nm)	$V_{3.5-10}$ (cm^3/g)	V_{10-50} (cm^3/g)	V_{50-150} (cm^3/g)	$V_{150-1000}$ (cm^3/g)	L_{macro} (nm)
0-Ref	13	0.008	0.020	3.3	0.004	0.000	0.008	0.052	-
7.9-Ref	34	0.020	0.083	5.5	0.026	0.039	0.001	0.019	-
0-3DOM	39	0.023	0.219	31.6	0.000	0.223	0. 287	0.137	42.5
0.8-3DOM	38	0.021	0.155	19.3	0.010	0.195	0.239	0.147	45.0
2.7-3DOM	39	0.022	0.133	16.1	0.010	0.125	0.112	0.135	53.2
7.9-3DOM	38	0.021	0.109	12.1	0.026	0.082	0.063	0.188	293.5
11.9-3DOM	37	0.020	0.077	8.1	0.030	0.029	0.026	0.166	269.4
15.9-3DOM	38	0.021	0.071	3.5	0.065	0.012	0.027	0.166	362.7

*Micropore and mesopore volume determined by Dubinin-Raduchkevich and BJH equations, respectively

**V_{X-Y}: pore volumes ranging from X to Y determined by Hg porosimetry

Table S2. Selectivity to CO (S_{CO}) at different soot conversions (Cx)

	S_{CO} (%)		
Sample	***C20***	***C50***	***C80***
No Catalysts	64.0	66.8	59.7
0-Ref	26.4	25.3	22.6
7.9-Ref	10.1	5.8	4.9
0-3DOM	8.1	5.3	3.0
0.8-3DOM	13.9	9.2	6.3
2.7-3DOM	6.0	4.8	5.6
7.9-3DOM	8.0	7.6	7.7
11.9-3DOM	11.7	8.5	8.2
15.9-3DOM	11.8	10.9	16.0

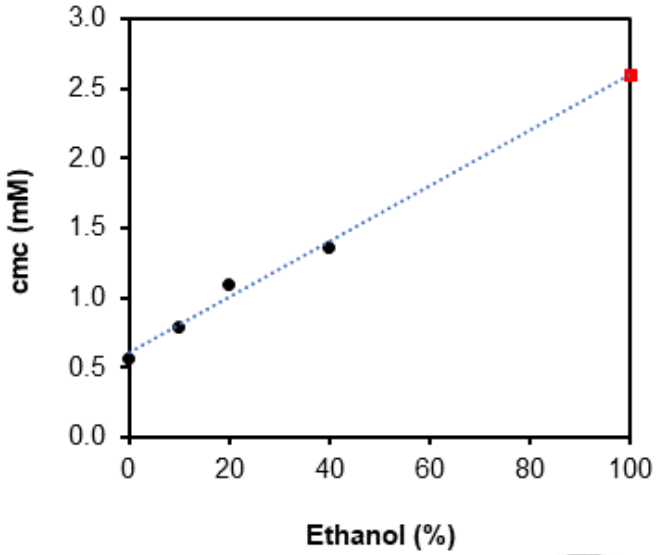

Figure S1. Critical micelle concentration (cmc) of F127 in different water-ethanol mixtures. (●) data from and (■) F127 estimated cmc in this study.

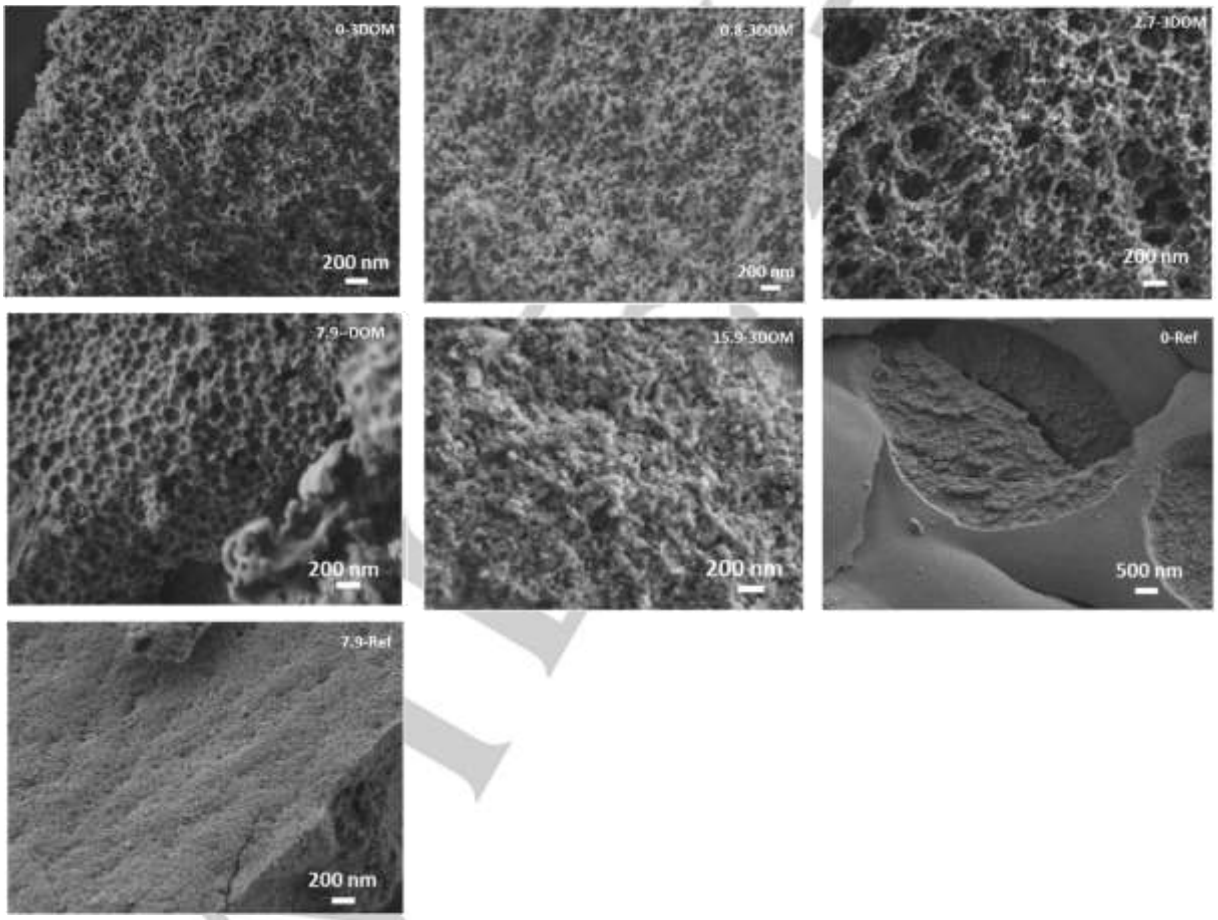

Figure S2. Magnified FESEM images of Ref and 3DOM catalysts

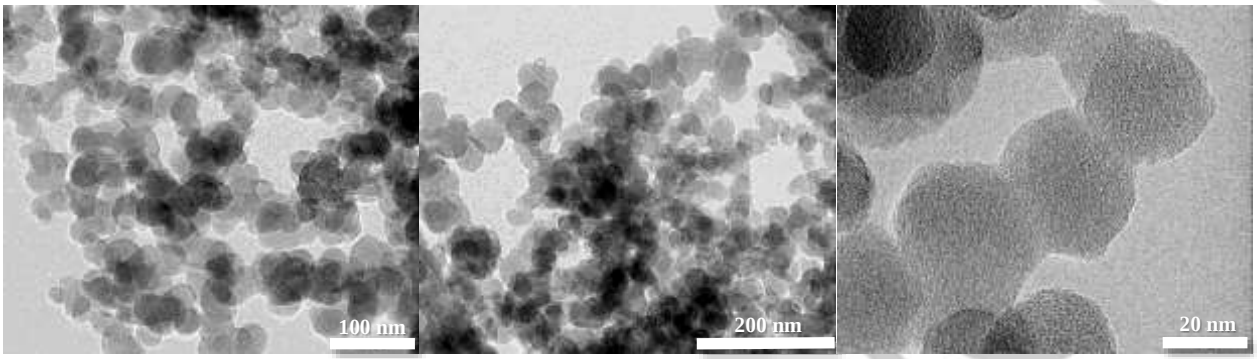

Figure S3. TEM images of soot (Printex U)